Iodine Intercalation in the Ionic Conductor $Sr_xBi_{9-x}O_{(27-x)/2}$

D. P. Scarfe and A. J. Jacobson*

Departments of Physics and Chemistry, University of Houston, Houston, Texas 77204-5641

Received June 11, 1997. Revised Manuscript Received August 26, 1997[⊗]

The intercalation reactions of iodine with the layered oxide ion conductors $Sr_xBi_{9-x}O_{(27-x)/2}$ (x = 0.90, 1.20, 1.50, 2.00, 2.40) have been studied by powder X-ray diffraction, thermogravimetric analysis, and Raman spectroscopy. X-ray diffraction data show that iodine atoms intercalate into the van der Waals gap between adjacent Bi−O sheets to form stage 1 compounds. The spacing between adjacent Bi−O layers increases by ∼3 Å corresponding to the intercalation of a monolayer of iodine atoms. The compositions and thermal stabilities of the intercalation compounds were determined by thermogravimetric analyses. Micro-Raman spectroscopy was used to show that the intercalated iodine species is predominantly I_3^-.

Introduction

Intercalation reactions are characterized by the insertion of a guest chemical species into a host lattice without major rearrangements of the host structure. These reactions often occur for highly anisotropic layered host materials where the interlayer coupling forces are substantially weaker than those of the intralayer ones (e.g., graphite[1] , transition metal dichalcogenides,[2] and more recently high-Tc superconductors[3]). Intercalation allows systematic investigation of charge transfer and anisotropic structural and electrical properties which can then be related to the host material.[1−7]

Recent examples of the use of intercalation reactions to study properties can be found in reactions of the high-T_c superconductors with different halogen-containing intercalants (Br_2, I_2, $HgCl_2$).[8−12] Intercalation reactions with the bismuth cuprate superconductors (e.g., $Bi_2Sr_2CaCu_2O_8$) in which iodine is intercalated between the square planar Bi−O sheets have been studied in some detail. Many different techniques, for example, Raman, EELS, XPS, and HRTEM,[4,10−16] have been used in order to determine the nature of the iodine species. Though some controversy remains, most of the evidence suggests that I_3^- is the predominant guest species.

We recently reported iodine intercalation in another type of layered bismuth oxide phase, rhombohedral $BaBi_8O_{13}$.[17] This host lattice is a good oxide ion conductor but is electronically insulating. Many structural analogues of $BaBi_8O_{13}$ exist in the phase diagrams of Bi_2O_3−MO (M = Ca, Sr, Ba),[18−23] Bi_2O_3−Ln_2O_3 (Ln = La, Sm, Gd),[18,24] and Bi_2O_3−Ln_2O_3−TeO_2 (Ln = La, Sm, Gd, Er).[25] The composition ranges of the rhombohedral phases containing alkaline earth and lanthanum cations have been most studied and compositions of the single phase regions have been determined: $Bi_{1-x}M_xO_{(3-x)/2}$ (M = Ca, x = 0.12−0.19; Sr, x = 0.10−0.27; Ba, x = 0.08−0.19) and in $Bi_{1-x}La_xO_{1.5}$ (x = 0.15−0.30). The high oxide ion conductivity has led to much interest in the rhombohedral Bi_2O_3 based solid solutions.[18−20] Typical ionic conductivities of these materials are $\sim 10^{-1}$ S cm^{-1} at 700 °C and 10^{-2}−10^{-3} S cm^{-1} at 500 °C,[18] approximately 1−2 orders of magnitude higher than those of the stabilized zirconias at the same temperatures. Recently, the possible transport pathways for O^{2-} diffusion were studied as a function of temperature by

* To whom correspondence should be addressed.

[⊗] Abstract published in *Advance ACS Abstracts,* October 15, 1997.

(1) *Graphite Intercalation Compounds 1*; Zabel, H., Solin, S. A., Eds.; Springer Series in Materials Science; Springer: New York, 1990.
(2) *Intercalation Chemistry*; Jacobson, A. J., Whittingham, M. S., Eds.; Academic Press: New York, 1982.
(3) Xiang, X−D.; McKernan, S.; Vareka, W. A.; Zettl, A.; Corkill, J. L.; Barbee, T. W. III; Cohen, M. L. *Nature* **1990**, *348*, 145.
(4) Xiang, X−D.; Vareka, W. A.; Zettl, A.; Corkill, J. L.; Cohen, M. L.; Kijima, N.; Gronsky, R. *Phys. Rev. Lett.* **1992**, *68*, 530.
(5) Huong; P. V.; Verma; A. L. *Phys. Rev. B* **1993**, *48*, 9869.
(6) Ha, D. H.; Lee, K. W.; Ri, H.-C.; Yoo, K. H.; Park, Y. K.; Oka, K.; Yamaguchi, Y.; Nishihara, Y. *Physica C* **1995**, *247*, 137.
(7) Pooke, D.; Kishio, K.; Koga, T.; Fukudam, Y.; Sanada, N.; Nagoshi, M.; Kitazawa, K.; Yamafugi, K. *Physica C* **1992**, *198*, 349.
(8) Liang, G.; Sahiner, A.; Croft, M.; Xu, W.; Xiang, X−D.; Badresingh, D.; Li, W.; Chen, J.; Peng, J.; Zettl, A.; Lu, F. *Phys. Rev. B* **1993**, *47*, 1029.
(9) Huong, P. V.; Pires, A.; Tomasini, S.; Wang, H.; Marquestaut, E. *Physica C* **1994**, *235−240*, 497.
(10) Buckley, R. G.; Staines, M. P.; Pooke, D. M.; Stoto, T.; Flower, N. E. *Physica C* **1995**, *248*, 247.
(11) Choy, J. H.; Kang, S−G.; Kim, D−H.; Itoh, M.; Inaguma, Y.; Nakamura, T. J. *Solid State Chem.* **1993**, *102*, 284.
(12) Stoto, T.; Pooke, D.; Kishio, K. *Phys. Rev. B* **1995**, *51*, 16220.
(13) Qiu, C. H.; Ahrenkiel, S. P.; Wada, N.; Ciszek, T. F. *Physica C* **1991**, *185*, 825.
(14) Faulques E.; Russo, R. E. *Solid State Commun.* **1992**, *82*, 531.
(15) Kishio, K.; Pooke, D.; Trodahl, H. J.; Subramaniam, C. K.; Kotaka, Y.; Seto, M.; Kitao, S.; Maeda, Y. J. *Superconductivity* **1994**, *7*, 117.
(16) Kijima, N.; Gronsky, R.; Xiang, X. D.; Vaseka, W. A.; Hou, J.; Zettl, A.; Corkill, J. L.; Cohen, M. L. *Physica C* **1992**, *198*, 309.
(17) Scarfe, D. P.; Bhavaraju, S.; Jacobson, A. *J. Chem. Commun.* **1997**, 313.
(18) Takahashi, T.; Iwahara, H; Nagai, K. *J. Appl. Electrochem.* **1972**, *2*, 97.
(19) Takahashi, T.; Esaka, T.; Iwahara, H. *J. Solid State Chem.* **1976**, *16*, 317.
(20) Conflant, P.; Boivin, J. C.; Nowogrocki, G.; Thomas, D. *Solid State Ionics* **1983**, *9−10*, 925.
(21) Conflant, P.; Boivin, J. C.; Thomas. D. *J. Solid State Chem.* **1976**, *18*, 133.
(22) Guillermo, R.; Conflant, P.; Boivin, J. C.; Thomas, D. *Rev. Chim. Miner.* **1978**, *14*, 153.
(23) Baek, H. D.; Virkar, A. V. *J. Electrochem. Soc.* **1992**, *11*, 139.
(24) Iwahara, H.; Esaka, T.; Sato, T.; Takahashi, T. *J. Solid State Chem.* **1981**, *39*, 173.
(25) Mercurio, D.; El Farissi, M.; Frit, B.; Réau, J. M.; Sénégas, *J. Solid State Ionics* **1990**, *39*, 297.

S0897-4756(97)00411-0 CCC: $14.00

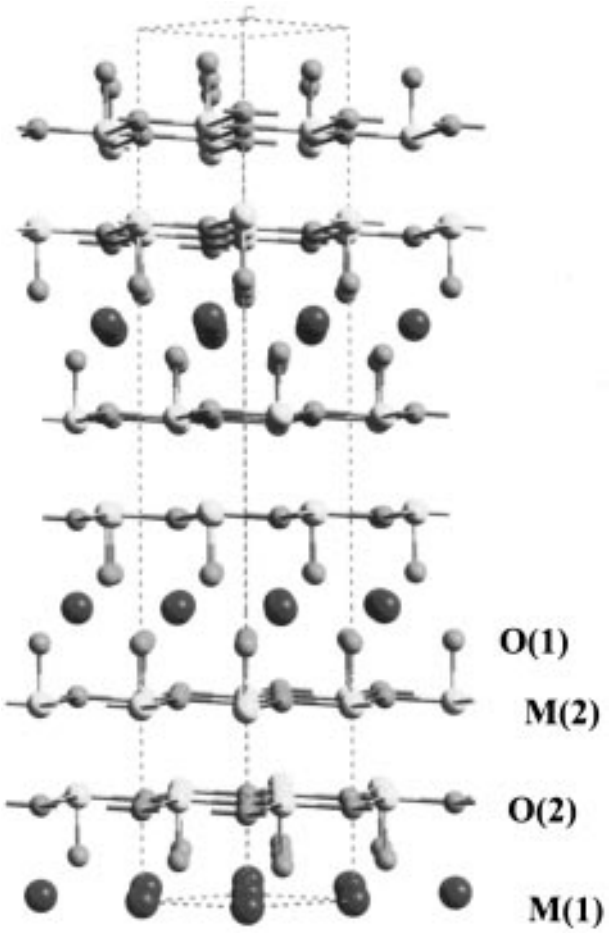

Figure 1. Structure of the rhombohedral phase host material.

single-crystal neutron diffraction.[26] Subsequently, iodine intercalation experiments confirmed that empty sites in the interlayer gap provide an essential transport pathway for rapid oxide ion diffusion in these compounds.[17]

The structure of the rhombohedral phase is shown in Figure 1 based on the single-crystal structure determination by Conflant et al.[27] The unit cell consists of three identical slabs, each made up from three metal oxide sublayers. These slabs are stacked in an ABC sequence separated by interlayer gaps to form one unit cell. This results in a unit cell with a stacking sequence ABC/BCA/CAB, where / indicates the interlayer gap between slabs and ABC or BCA or CAB separately indicates the stacking of the metal oxide sublayers within each slab. There are two inequivalent metal sites: M(2) is the metal site directly adjacent to the interlayer gap and is fully occupied by bismuth atoms; the M(1) site is in the middle of a slab and is also fully occupied but contains both Bi and Sr cations in a ratio determined by the specific stoichiometry. There are a total of three oxygen sites: O(2) is almost coplanar with Bi(2) and forms a slightly distorted hexagonal Bi(2)−O(2) sheet. The O(1) anion lies within the slab and is coordinated to a Bi(2) atom completing the 4-fold coordinated BiO_4 unit. The M(1) site has a 6 + 2 8-fold coordination environment. Additional O(3) anions occupy sites in the plane of the Bi(2)−O(2) layers with a low occupancy (0.2−0.3) and are located near the center of the hexagons formed by the Bi(2) and O(2) atoms.

Variations in the divalent to trivalent (Sr^{2+}/Bi^{3+}) cation ratio result in a corresponding change in the oxygen stoichiometry. Changes in the Sr/Bi ratio are apparently accommodated by the lattice in the following way:[20,27−30] the O(1) site remains fully occupied, whereas the O(2) and O(3) sites have varying occupancies according to the Sr^{2+}/Bi^{3+} (divalent/trivalent) cation ratios (with O(2) and O(3) occupancies of ∼0.8−0.95, and ∼0.2−0.3, respectively). The $Bi_{1-x}La_xO_{1.5}$ structure is unique in that an additional partially occupied oxygen site (O(4)) is located in the interlayer gap between the Bi−O sheets. In the compounds containing divalent cations, no oxygen atoms are found within the interlayer gap.

In this paper we present a systematic study of iodine intercalation reactions with the rhombohedral oxide ion conductor $Sr_xBi_{9-x}O_{(27-x)/2}$ for a series of compositions (x = 0.90, 1.20, 1.50, 2.00, 2.40). The intercalation reactions have been studied using powder X-ray diffraction (XRD), thermogravimetric analysis (TGA), and Raman spectroscopy. The location of the iodine layer within the host material and the nature of the iodine species have been determined. The stoichiometries of the intercalation compounds have also been related to the Bi/Sr ratios in the host lattices.

Experimental Section

The host compounds were synthesized by reactions of stoichiometric amounts of high purity $SrCO_3$ (99.995%) and Bi_2O_3 (99.999%) obtained from Aldrich Chemical Co. The reactants were mixed and then heated at 775 °C in air for 15−20 h. Several cycles of regrinding and reannealing were carried out (typically three) until powder X-ray diffraction patterns showed that the products were single phase.

The intercalation reactions were carried out by encapsulating the host material and excess I_2 in an evacuated (∼50 mTorr) Pyrex tube. The amount of excess iodine was varied from ∼4 to 5 mol I_2 per mole of Sr−Bi−O so that the same iodine pressure of ∼5 atm was attained at the beginning of each reaction. All reactions were carried out in a horizontal tube furnace at a temperature of 215 °C. The reactions were allowed to proceed for 3 days. The tube was then repositioned so that one end was at room temperature and the other at 215 °C. The excess iodine was sublimed to the cool end over a period of 2 days. The total reaction sequence was carried out three times with intermediate grinding of the products to ensure complete reaction and that the host material had been saturated with iodine at the reaction temperature. After removal of the excess iodine the compounds changed color from yellow to brown on intercalation. The intercalation reactions were found to be quite sensitive to both the reaction temperature and the time used to sublime off the excess I_2. Reproducible data were obtained only after the extended reaction times (∼9 days total) and long I_2 sublimation times (6 days total) described above. All results reported below used the same synthesis procedure so that results for compounds with different Bi/Sr ratios can be compared.

Powder X-ray diffraction (XRD) measurements were made using a Scintag XDS2000 automated diffractometer with copper Kα radiation ($\theta-\theta$ mode, flat plate geometry, $2° \leq 2\theta \leq 65°$). Electron microprobe analyses were performed on a JEOL JXA-8600 operated at 15 keV using wavelength dispersive spectrometers. Weight loss measurements were made with a DuPont 2950 thermogravimetric analyzer. The TGA experiments were carried out in a flowing N_2 atmosphere saturated with water at ambient temperature. Samples were heated to 700 °C at 5 °C/min and then held at this temperature

(26) Mercurio, D.; Champarnaud-Mesjard, J. C.; Frit, B.; Conflant, P.; Boivin, J. C.; Vogt, T. *J. Solid State Chem.* **1994**, *112*, 1.
(27) Conflant, P.; Boivin, J. C.; Thomas, D. *J. Solid State Chem.* **1980**, *35*, 192.

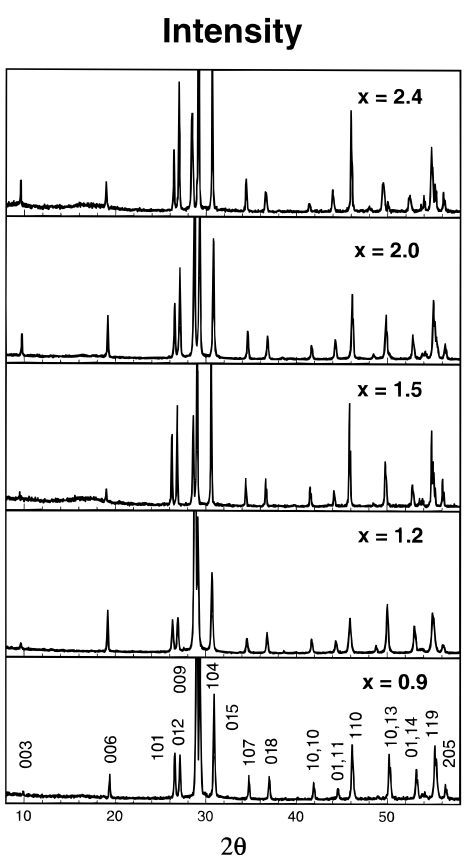

Figure 2. Powder X-ray diffraction patterns of the $Sr_xBi_{9-x}O_{(27-x)/2}$ host materials.

for 12 h. The micro-Raman spectra were recorded at room temperature using a commercial microoptical system (I.S.A. Model S3000). The 514.5 nm line from an argon ion laser was used as the excitation source and a silicon diode array was used as the photodetector. A sampling area of approximately 1 μm^2 was obtained by focusing the laser beam with a 100× microscope lens.

Results

X-ray Diffraction. The powder X-ray diffraction data of the starting materials were completely indexed with rhombohedral unit cells. The data were refined using the Rietveld method by using the program GSAS with hexagonal axes.[31] The starting parameters for the refinements were based on the published single-crystal data in space group $R\bar{3}m$.[26,27] The refinements indicated some preferred orientation along the *c* direction (hexagonal indexing) and the refinements were used only to obtain lattice constants. The indexed powder XRD patterns of the host materials are shown in Figure 2a−e and the refined lattice parameters are given in Table 1. The powder XRD patterns of the corresponding iodine intercalation compounds are shown in Figure 3a−e. These diffraction patterns show a series of 00*l* peaks shifted to lower angles indicating an expansion of the unit cell along the *c* axis. The diffraction patterns of the intercalation compounds were indexed with similar unit cells to the host compounds but with an expansion

Table 1. Lattice Parameters for the Host Lattices and Intercalation Compounds Calculated from Refinements of the Powder XRD Data

	host material		intercalation compound	
composition	*a* (Å)	*c* (Å)	*a* (Å)	*c* (Å)
$Sr_{0.90}Bi_{8.10}O_{13.05}$	3.9642(3)	28.105(2)	3.998(2)	36.992(5)
$Sr_{1.20}Bi_{7.80}O_{12.90}$	3.9648(5)	28.104(2)	3.995(4)	37.195(9)
$Sr_{1.50}Bi_{7.50}O_{12.75}$	3.9644(2)	28.193(2)	3.999(2)	37.525(10)
$Sr_{2.00}Bi_{7.00}O_{12.50}$	3.9674(4)	28.372(2)	3.996(5)	37.662(8)
$Sr_{2.40}Bi_{6.60}O_{12.30}$	3.9697(2)	28.566(2)	4.001(3)	37.967(6)

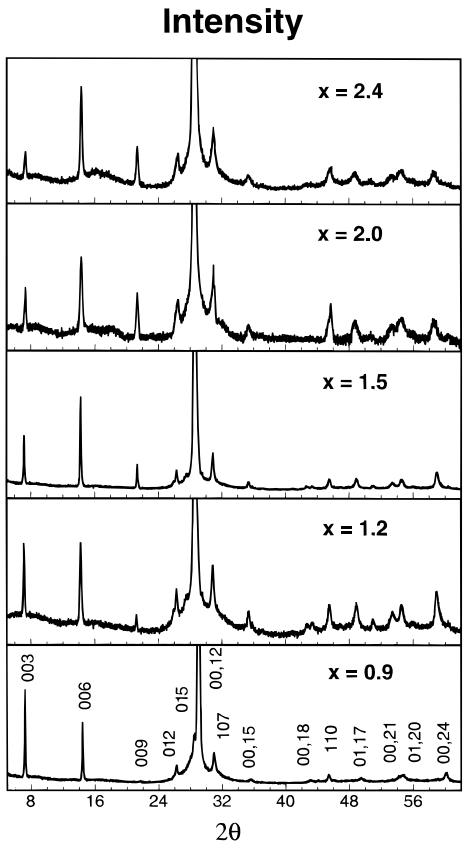

Figure 3. Powder X-ray diffraction patterns of the $I_ySr_xBi_{9-x}O_{(27-x)/2}$ intercalation compounds.

along the *c* axis of ~9 Å. The 00*l* peaks are much more intense than the *hkl* peaks, probably due to an increase in preferred orientation as the material becomes increasingly anisotropic upon intercalation. However, in-plane disorder of the intercalant or disorder in the stacking sequence of slabs may contribute somewhat to the reduction and broadening of the *hkl* intensities. No superlattice reflections that would indicate in-plane ordering of I_3^- ions were observed.

A noticeable difference is observed between the XRD patterns of the host materials and of the intercalation compounds. The intensities of the 003, 006, and 009 peaks for the intercalation compounds systematically change as the Sr/Bi ratio is varied (the 003 peak decreases while the 006 and 009 peaks increase as the Sr content increases). The variation may be due to either differences in iodine stoichiometries or the change in ratio of Sr/Bi on the M(1) site or a combination. To understand the location and occupancy of the iodine atoms within the intercalation compounds, the 00*l* peak intensities were calculated with a model in which a monolayer of iodine is inserted in the van der Waals gap midway between hexagonal Bi(2)−O(2) sheets in adjacent slabs (stage 1 structure). The intensities were

(28) Boivin, J. C.; Thomas, D. *Solid State Ionics* **1981**, *5*, 523.
(29) Blower, S. K.; Greaves, C. *Mater. Res. Bull.* **1988**, *23*, 765.
(30) Mercurio, D.; El Farissi, M.; Champarnaud-Mesjard, J. C.; Frit, B.; Conflant, P. Foult, G. *J. Solid State Chem.* **1989**, *80*, 133.
(31) Larson, A. C.; von Dreele, R. B. GSAS Users Guide, Los Alamos National Laboratory, Los Alamos, NM, 1990.

Table 2. Iodine Contents, *y*, in $I_ySr_xBi_{9-x}O_{(27-x)/2}$, and the Iodine Weight Losses (Δy) after Completion of Each Step Calculated from the TGA Data

Composition	*y* (XRD)	*y* (TGA)	$\Delta y(1)$	$\Delta y(2)$	$\Delta y(3)$
$Sr_{0.90}Bi_{8.10}O_{13.05}$	3.1(1)	2.80	0.55	0.66	1.59
$Sr_{1.20}Bi_{7.80}O_{12.90}$	3.1(1)	3.01	0.68	0.70	1.63
$Sr_{1.50}Bi_{7.50}O_{12.75}$	3.2(1)	3.12	0.87	0.72	1.53
$Sr_{2.00}Bi_{7.00}O_{12.50}$	3.3(1)	3.39	1.01	0.89	1.49
$Sr_{2.40}Bi_{6.60}O_{12.30}$	3.5(1)	3.51	1.28	0.95	1.28
$Ba_{1.00}Bi_{8.00}O_{13.00}$		2.83	0.46	0.61	1.76

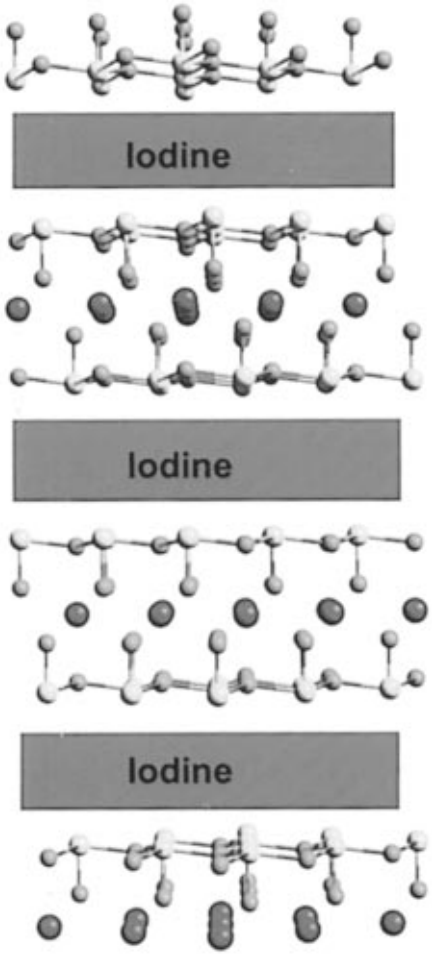

Figure 4. Schematic structural illustration of the iodine intercalation compounds.

modeled by varying the scale factor, the iodine atom occupancy, and thermal parameters. The iodine contents determined from the comparison of the observed and calculated intensities are given in Table 2. Structure factor calculations indicated that the variation in intensities of the low-angle 00*l* peaks is mostly due to the different Sr/Bi ratios on the M(1) site in the intercalation compounds. The refined lattice parameters for the intercalation compounds are given in Table 1. A large increase in the *c* axis spacing is observed upon intercalation whereas the in-plane lattice parameter increases by only a small amount but is the same within error for the different intercalation compounds. A schematic illustration of the resulting intercalation compound is given in Figure 4.

Thermogravimetric Analysis. Thermogravimetric analyses (TGA) were used to determine the thermal stability and iodine content of the intercalation compounds. Previously, we have used TGA to analyze the $I_yBaBi_8O_{13}$ and shown that this technique gives reliable

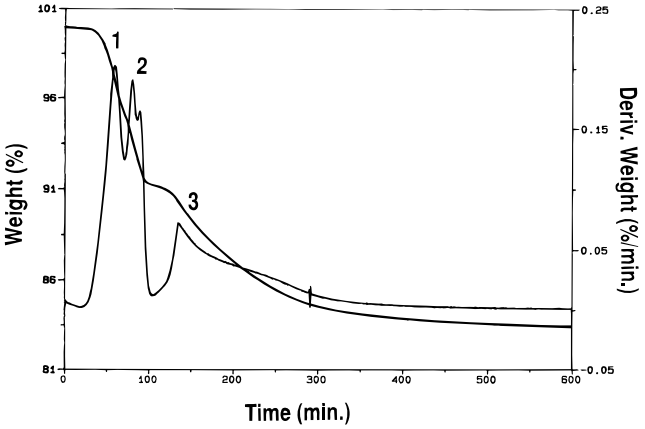

Figure 5. Typical TGA data for the intercalation compounds. Three weight loss steps (labeled 1, 2, 3) are indicated by peaks in d*w*/d*T* (weight change with respect to temperature).

results for iodine contents.[23] We have also used electron microprobe analysis (EMPA) but find that this technique often induces some beam damage since the compounds are electronic insulators. Where little beam damage occurs, EMPA and TGA agree well but in general for these particular systems the EMPA data were less reproducible. Consequently, the TGA data were used to determine the iodine contents of the different Sr/Bi ratio intercalation compounds.

A typical TGA curve for an intercalation compound (Figure 5) displays three steps in the weight loss (labeled 1, 2, 3 in Figure 5) indicated by the maximum in the derivative of the weight change with respect to temperature. To understand the origin of these different steps, samples were cooled in the TGA furnace to room temperature at the end of the temperature range for each respective step. Powder XRD patterns of the samples recovered were then used to identify the reaction products.

After step 1, which occurs from 240 to 400 °C, the powder XRD patterns show a clear set of 00*l* peaks similar to those of the initial sample. The weight loss is therefore assigned to deintercalation of iodine from each layer. The weight losses at the end of step 1 are given in Table 2 for the compounds with different Sr/Bi ratios. XRD patterns of the material recovered after heating to the end of step 2 indicate that the intercalation compounds decompose below 600 °C. The XRD data show that the unintercalated host lattice is the majority phase but the reaction product also contains other unidentified phases. Annealing the sample at 700 °C (step 3) for 12 h results in a leveling off of the weight to a constant value. XRD patterns after this heat treatment show the formation of single phase starting material. The weight difference between the intercalation compound and the final product was used to determine the iodine stoichiometry.

Micro-Raman. Many systematic investigations have been reported for the Raman spectra of iodine species.[32−35] These studies provide a method by which to identify possible iodine configurations within a molecule or crystal structure. Figure 8a−c show Raman spectra of the iodine intercalated samples with $x = 0.90$, 1.50, 2.40 at room temperature. The spectra are very similar to those observed in iodine intercalated $Bi_2Sr_2CaCu_2O_8$[20,21] and also in other molecules which contain I_3^- ions.[32−35] From Figure 6 it is clear that even though

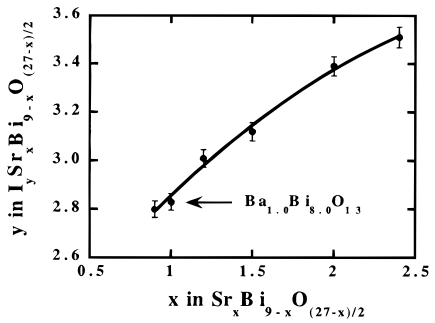

Figure 6. Variation of the iodine stoichiometry with composition x $Sr_xBi_{9-x}O_{(27-x)/2}$.

the stoichiometry of the host material is different for each sample, the Raman line intensities and line positions remain invariant and are presumed to arise from the vibrational modes of the intercalated iodine species. The strongest line which occurs at 102 cm^{-1} can be assigned from the literature data to the symmetric stretching mode (ν_1) of the linear I_3^- ion. A harmonic of the 102 cm^{-1} symmetric stretching mode is also observed at approximately 207 cm^{-1} ($2\nu_1$) and is rather broad and weak. Another line occurring at 149 cm^{-1} can be assigned to the asymmetric stretch (ν_3) of this I_3^- ion. The broad nature of all three peaks may be associated with disorder of the iodine atoms within the layer as suggested by the XRD data. The identification of I_3^- as the intercalated species indicates that charge transfer is associated with the intercalation process.

Discussion

A series of new intercalation compounds have been obtained by reaction of iodine with the layered oxide ion conductors $Sr_xBi_{9-x}O_{(27-x)/2}$ ($x = 0.90$, 1.20, 1.50, 2.00, 2.40). The X-ray diffraction data show that the iodine intercalation results in a lattice expansion along the *c* axis of ~9 Å for each hexagonal unit cell or ~3 Å for each van der Waals gap. The *c* axis spacings increase slightly from 8.9 to 9.4 Å over the range of compositions studied. The *a* axes spacings are little altered from those of the starting materials and are almost invariant with Sr/Bi ratio. Refinements of the 00*l* intensities indicate the formation of stage one compounds which contain a monolayer of iodine between Bi−O layers. The refinements give iodine compositions in good agreement with the TGA results (see below and Table 2). An increase in structural disorder on intercalation can be seen by comparison of the diffraction patterns shown in Figures 2 and 3. The disorder is apparent both in the line widths and in the diminished intensities of the higher angle reflections. Some mixed reflections are, however, still observed and all reflections obey rhombohedral absences suggesting that the Sr−Bi−O layer stacking is unaltered on intercalation of iodine atoms. The diffraction data show no evidence for any in-plane ordering of the guest species.

The iodine contents calculated from weight losses of the respective compounds are given in Table 2. For the synthesis conditions chosen in this study, the amount of iodine intercalated systematically increases as the Sr occupation of the M(1) site increases as shown in Figure 6. Previous experiments have shown that the iodine content is variable and depends on the synthesis conditions used. In our previous study under different synthesis conditions, we obtained a compound with the composition $I_{3.1}BaBi_8O_{13}$ compared to $I_{2.83}BaBi_8O_{13}$ obtained in the present study. On heating to 400 °C, all of the compounds lose some iodine but without destruction of the intercalation compound. The compositions obtained after heating to 400 °C correspond to $I_{1.30\pm0.07}Sr_xBi_{9-x}O_{27-x}$ suggesting a limiting composition that is independent of the Sr content. The compositions determined at the end of this first step have some uncertainty because the end of the step is marked only by a minimum in the derivative and not by a definite plateau. Further heating results in continued deintercalation together with decomposition and the formation of other phases. The starting host materials are only re-formed from these intermediates by heating at higher temperatures for long times.

Table 3. Relation between the Difference in Oxygen Vacancy Content and the Difference in the Amount of Intercalated Iodine Per Unit Cell

composition	Δ[O(2) + O(3)]	ΔI_{total}
$Sr_{0.90}Bi_{8.10}O_{13.05}$		
$Sr_{1.20}Bi_{7.80}O_{12.90}$	0.15	0.21
$Sr_{1.50}Bi_{7.50}O_{12.75}$	0.30	0.32
$Sr_{2.00}Bi_{7.00}O_{12.50}$	0.55	0.59
$Sr_{2.40}Bi_{6.60}O_{12.30}$	0.75	0.71
$Ba_{1.00}Bi_{8.00}O_{13.00}$	0.05	0.03

Micro-Raman spectroscopy shows clear evidence for the presence of I_3^- in the intercalation compounds though the Raman bands are broad, indicating disorder and possibly the presence of other species such as I_5^-. The Raman data confirm that the intercalation mechanism involves electron transfer from the host to the guest species. This is also suggested by the stability of the intercalation compounds. The reduction of iodine on intercalation to form I_3^- requires a corresponding mechanism for oxidation of the host lattice. The details of this are less certain. The creation of holes on either the Bi sites ($Bi^{3+} \rightarrow Bi^{5+}$) or the oxygen sites ($O^{2-} \rightarrow O^-$) within the metal oxide layers are the likely alternatives.

In considering possible host oxidation mechanisms, it is of interest to examine the variation of the iodine content with the composition of the host lattice. The iodine content increases with increasing strontium atom content as shown in Figure 6. The increase in iodine content decreases as the Sr content increases, suggesting a trend toward a saturation value determined by the packing density of iodine atoms within the van der Waals gap. It is difficult to estimate precisely the value of the saturation coverage because it depends on the packing model chosen and on the chemical nature of the intercalated species. Assuming that I_3^- is the only species present, we estimate a maximum iodine content of 4.3 consistent with the general trend in Figure 6. For a model in which the centers of each I_3^- are located over the bismuth atoms in the host layer, a composition of 1.3−1.5 is estimated depending on the in-plane arrangement. This value is close to the value obtained at 400 °C for all compositions. The general increase in the iodine content observed with increasing Sr content may reflect the increasing ease of oxidation of the host lattice as the content of the more basic cation, strontium increases.

We note that there is a correlation between the iodine content and the occupancy of the O(2) and O(3) sites.

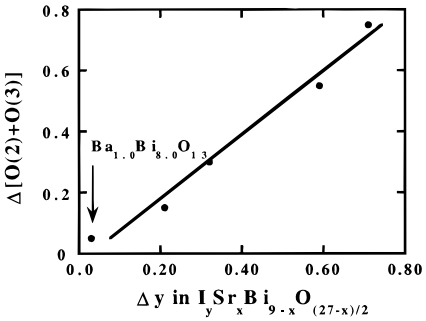

Figure 7. Variation in the amount of intercalated iodine and the change in oxygen vacancy concentration (O(2) + O(3)).

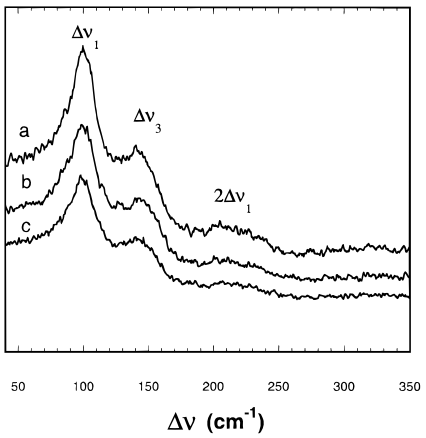

Figure 8. Micro-Raman spectra of the iodine intercalation compounds $I_ySr_xBi_{9-x}O_{(27-x)/2}$: (a) $x = 0.90$; (b) $x = 1.50$; (c) $x = 2.40$.

The O(2) + O(3) sites have variable occupancy and sit in the hexagonal Bi−O sheet and are adjacent to the layer of intercalated iodine atoms. The increase in Sr content in the host lattice is accommodated by increasing the number of vacancies in the O(2) and O(3) sites. With reference to the compound with $x = 0.90$, the increase in iodine content of the compounds with other Sr/Bi ratios with $x > 0.90$ depends almost linearly on the O(2) + O(3) site occupancies (Table 3 and Figure 7) as anticipated from the general trend in Figure 6. The composition of a sample of intercalated $BaBi_8O_{13}$ prepared by an identical heat treatment is also shown in Figure 7. The fact that both Sr and Ba compounds follow the same correlation suggests that there may be a direct relation between the in-plane oxygen content and the oxidation mechanism. A mechanism that involves the fomation of a peroxide species involving O(2) and O(3) could account for this relationship. Peroxide species have been previously suggested to occur on oxidation of compounds such as La_2NiO_{4+x} and La_2CuO_{4+x}.[36,37]

Summary and Conclusions

Iodine intercalation compounds of the layered oxide ion conductors $Sr_xBi_{9-x}O_{(27-x)/2}$ ($x = 0.90$, 1.20, 1.50, 2.00, 2.40) have been synthesized. X-ray diffraction data show that iodine atoms intercalate into the van der Waals gap between adjacent Bi−O sheets to form stage 1 compounds. The spacing between adjacent Bi−O layers increases by ∼3 Å corresponding to the intercalation of a monolayer of iodine. Micro-Raman spectra indicate that the intercalated iodine species are I_3^- and that, therefore, intercalation involves charge transfer and oxidation of the host lattice. Further studies are in progress in order to examine the mechanism of charge transfer from the host lattice and to investigate the in-plane ordering of the intercalated iodine species by single-crystal diffraction studies.

Acknowledgment. We thank the Texas Center for Superconductivity and the Robert A. Welch Foundation for financial support of this work and B. Lorenz for help in obtaining the Raman data. The work was supported in part by the MRSEC program of the National Science Foundation under Award No. DMR-9632667.

CM970411N

(32) Gabes, W.; Gerding, H. *J. Mol. Struct.* **1972**, *14*, 267.
(33) Mulazzi, E.; Lefrant, S.; Perrin, E.; Faulques, E. *Phys. Rev. B* **1987**, *35*, 3028.
(34) Bernard, M.; Rzepka, E.; Lefrant, S. *Nucl. Instrum. Methods Phys. Res.* **1990**, *B46*, 235.
(35) Andrews, L.; Prochaska, E. S.; Loewenschuss, A. *Inorg. Chem.* **1980**, *19*, 463.
(36) Chaillout, C.; Chenevas, J.; Cheung, S. W.; Fisk, Z.; Marezio, M.; Morosin, B.; Schirber, J. E. *Physica C* **1990**, *170*, 87.
(37) Grenier, J. C.; Wattiaux, A.; Monroux, C.; Pouchard, M; Locquet, J. P. *Physica C* **1994**, *235−240*, 79.